Politecnico di Milano
School of Industrial and Information Engineering
Master of Science in Aeronautical Engineering
Department of Aerospace Science and Technology

Design and optimization tool for multirotor unmanned aerial vehicles

Advisor: Prof. Marco LOVERA
Co-Advisor: Ing. Mattia GIURATO

Thesis by:
Eril BALCIOGLU Matr. 874373

Academic Year 2018–2019

Acknowledgments

There are many people who I personally want to thank for supporting me during the course of this thesis.

First of all, I would like to express my great appreciation to Professor Marco Lovera for all his trust, inspiration and guidance. His aid and suggestions have been fundamental.

Secondly, I would like to thank Mattia Giurato for his valuable support and lead throughout the development of this thesis.

Also, I thank all the members of Aerospace Systems & Control Laboratory for their help and hospitality during the process.

Furthermore, a lot of thanks go to my friends in and out of Italy that stood by my side on every occasion. I really appreciate the unconditional support that I received from you.

Finally, special thanks go to my family for giving me the opportunity and encouragement to live this experience. Without you, all of my work would become worthless.

Abstract

Currently, multirotor unmanned aerial vehicles cover a broad area of the aeronautical field of applications and have the clear opportunity to grow more and more in the near future. Besides the aeronautical part that they contain, their occupation in various fields of computer science, automation, control, and aerospace makes these platforms very valuable but challenging to work on. Such vehicles provide solutions to many areas such as e.g., security, surveillance, agriculture, civil monitoring, filming, and photography.

Despite numerous ongoing researches and developments on multirotor UAV platform design processes, there is no wide range of options that generate a systematic, software-based approach. Still today, most of the multirotor UAV designers use the heuristic approach to construct these platforms. These design procedures can only take advantage of previously constructed, similar platforms' data and can be validated through experimental procedures without preliminary aerodynamic and electrical analyses.

Furthermore, the researches that focus on the parametrization of multirotor UAV components revealed a basic and effective way to describe their physical and electrical characteristics. Despite these findings, there are no more than one tool on the market that takes advantage of the parametrization techniques to estimate component characteristics and makes detailed analyses.

The main goal of this thesis is to develop a tool that uses both inductive and deductive approaches to design a multirotor UAV while considering the basic aerodynamic and electrical properties of the constitutive components. In detail, a combined tool containing two different approaches has been developed to address the design problem of multirotor UAVs, especially taking the performance requirements into consideration. In addition, the parametrization techniques for estimating the physical and electrical properties of the vehicle components are used in the tool.

Sommario

Gli UAV (aeromobili a pilotaggio remoto) multirotore coprono ad oggi un'ampia gamma di applicazioni in campo aeronautico e hanno grandi possibilità di ulteriore sviluppo in un prossimo futuro. Oltre alla componente strettamente aeronautica propria di queste tecnologie, il loro impiego in numerosi campi dell'informatica, dell'automazione, del controllo e in ambito aerospaziale rende queste piattaforme di grande valore, ma presenta anche diverse problematiche. Questi veicoli forniscono soluzioni in diverse aree tra cui sicurezza, sorveglianza, agricoltura, monitoraggio civile, fotografia e cinematografia.

Nonostante le numerose ricerche e lo sviluppo di processi di progettazione delle piattaforme UAV multirotore, non esiste una tale gamma di opzioni che generi un approccio sistematico e implementabile. Ad oggi, la maggior parte dei progettisti di UAV multirotore impiega approcci euristici per costruire queste piattaforme. Queste tipologie di procedure possono unicamente appoggiarsi a dati di piattaforme simili realizzate in precedenza e possono essere validate attraverso procedure sperimentali, senza analisi aerodinamiche ed elettriche preliminari.

Inoltre, le ricerche inerenti alla parametrizzazione di componenti di UAV multirotore hanno rivelato un modo semplice ed efficace, anche se approssimato, per descrivere le loro caratteristiche fisiche ed elettriche. Nonostante tali risultati, ad oggi è presente sul mercato solamente uno strumento che trae vantaggio dalle tecniche di parametrizzazione per stimare le caratteristiche dei componenti e produrre analisi dettagliate in fase di progettazione.

L'obiettivo principale di questa tesi è lo sviluppo di un tool che utilizzi approcci induttivi e deduttivi per la progettazione di un UAV multirotore, considerando le caratteristiche aerodinamiche di base e quelle elettriche dei componenti costitutivi. In dettaglio, un tool combinato di due diversi approcci è stato sviluppato per supportare il design di UAVs multirotore, tenendo particolarmente in considerazione i requisiti di performance. In aggiunta, le tecniche di parametrizzazione per la stima delle proprietà fisiche ed elettriche dei componenti del veicolo sono impiegate nel tool.

Contents

Introduction **1**

1 Component parametrization **3**
1.1 Drive components . . . 3
1.1.1 Electric motors . . . 3
1.1.2 Electronic Speed Controllers (ESCs) . . . 4
1.1.3 Batteries . . . 4
1.1.4 Propellers . . . 5
1.2 Mass parametrization of drive components . . . 5
1.2.1 BLDC motor . . . 5
1.2.2 ESC . . . 6
1.2.3 LiPo battery . . . 6
1.2.4 Propeller . . . 8
1.2.5 Mass breakdown . . . 10

2 Propeller modeling **11**
2.1 Rotor aerodynamics . . . 11
2.1.1 Momentum Theory . . . 11
2.1.2 Blade Element Theory (BET) . . . 14
2.1.3 Blade Element Momentum Theory (BEMT) . . . 17
2.2 Geometric parametrization of the propeller . . . 18
2.2.1 Chord & twist distribution . . . 18
2.2.2 Airfoil selection . . . 19

3 Design and optimization tool **21**
3.1 Forward Design tool . . . 21
3.1.1 Inputs . . . 21
3.1.2 Electrical model . . . 24
3.1.3 BEMT algorithm . . . 26
3.1.4 Performance analyses . . . 26
3.1.5 Sensitivity analyses . . . 28
3.2 Drive Optimizer . . . 28
3.2.1 Inputs . . . 30

3.2.2 Algorithm 31
3.3 Computational effort 32

4 Results **33**
4.1 Mass estimation survey 33
4.2 Forward Design tool results 34
4.2.1 Design tools on the market 34
4.2.2 Comparison with ancestor tools 35
4.2.3 Comparison with experimental flight data 35
4.2.4 Forward flight comparison between FDT & EMST 37
4.2.5 Sensitivity analyses scheme 37
4.2.6 Reasons of inaccurate results 38
4.3 Drive Optimizer results 39

Conclusions **43**

Bibliography **46**

List of Figures

1.1 Motor speed constant vs. mass[4] 6
1.2 Motor speed constant vs. mass with modified OR fit[4] 7
1.3 ESC maximum rated amperage vs. mass[4] 7
1.4 Battery capacity vs. mass[4] 8
1.5 Propeller diameter vs. mass[4] 9

2.1 Flow model of a rotor in hovering flight[13] 12
2.2 Flow velocities and aerodynamic setting of a blade element[13] . . . 15
2.3 Geometric data of GWS SlowFly 11x4.7[5] 18
2.4 Twist of GWS propellers at 0.6R with respect to different propeller pitch values[4] 19

3.1 Overview of FDT 22
3.2 Motor internal resistance to zero-load current[10] 24
3.3 Circuit model of the developed tool 26
3.4 Overview of DO 29

List of Tables

1.1 Parameters in equation (1.4) for different propeller materials . . . 9

4.1 Mass estimation survey . . . 34
4.2 UAV configurations used in the survey . . . 35
4.3 FDT hover endurance comparison with other tools . . . 36
4.4 Hover endurance differences between the tools for the survey in Table 4.3 . . . 36
4.5 FDT hover endurance results compared with experimental flight data 36
4.6 eCalc hover endurance results compared with experimental flight data . . . 37
4.7 3DR Iris+ forward flight comparison . . . 37
4.8 Quad Mini Generic forward flight comparison . . . 38
4.9 Sensitivity analyses for ASCL ANT-1 . . . 38
4.10 ANT-R compared with DO results . . . 39
4.11 TILT-X compared with DO results . . . 40
4.12 CARRIER-1 compared with DO results . . . 40
4.13 ANT-R compared with DO results operated in "constrained motor" mode . . . 40
4.14 Lower bound example scheme of DO . . . 41
4.15 Performance requirements and assumptions of lower bound example in Table 4.14 . . . 41

Introduction

Multirotor UAVs are aerial vehicles that have multiple rotors driven by electric motors. These vehicles are capable to hover and maneuver in the air and controlled by the thrust generated by each rotor.

The most important part of designing a multirotor unmanned aerial vehicle is the selection of the so-called "drive components". These components, which are the electric motors, electronic speed controllers (ESCs), batteries and propellers, are the most significant parts that affect the performance. There are several aspects that need to be considered during the selection of these components to achieve the desired performance.

At present, the most used approaches to select the drive components are based on previously built multirotor configurations and the component data notified by the manufacturer, which may be inaccurate. These design procedures may shift away from the actual requirements that the designed vehicle must satisfy. So, an appropriate design method should be developed to cover all the performance requirements of the built vehicle.

Currently, a variety of design methods have been proposed by several academics. A design process to select the drive components that makes use of Blade Element Momentum Theory is proposed by Latorre[12], but it does not perform an optimization regarding performance objectives. Bershadsky[4] documents a parametrization technique to estimate the masses of the drive components and a design tool to size the propulsion system of a multirotor UAV. This thesis makes use of the same mass estimation process combined with BEMT and electrical parametrization techniques reported by Gur[10] and Ampatis[2] to develop a design and optimization tool for multirotor UAVs, which mainly eliminates the need of a database for the drive components and contains the capability to optimize a configuration that takes into account the performance requirements for the vehicle in-design.

Thesis Description

The goal of this thesis is to develop a tool that has two different approaches to design a multirotor UAV.

The first approach, which can be named as an inductive analysis approach, is to estimate the performance capabilities of the vehicle by the prescribed drive

components. The second approach, which is a deductive design approach, is to find a suitable configuration which is able to achieve the prescribed performance and weight requirements. These two approaches can be considered as antipoles and one can be used to validate the other.

Thesis Structure

The parts of the thesis are listed below:

- In Chapter 1, the drive components, their importance and how to estimate their masses by previously proposed techniques in literature are introduced.
- Modeling technique of a multirotor propeller for the analyses containing the applicable aerodynamic theories to the rotor platform is documented in Chapter 2
- Algorithms of the developed tool are explained in Chapter 3
- In Chapter 4, the results of the mass estimation procedure compared with the real mass of the components and the results of the proposed tool, which are also compared with the two other design tools and experimental flight data are reported.

Chapter 1

Component parametrization

Multirotor unmanned aerial vehicle drive systems involve four components; electric motors, electronic speed controllers (ESCs), batteries and propellers. These four components can be named as *drive components*, the necessary parts of a multirotor UAV to fly. The selection of these components is the main consideration while designing a multirotor vehicle to achieve the desired performance capabilities.

Parametrizing drive components to estimate the total capability of multirotors is the principal design consideration for UAV applications. These components have one or more parameters that describe their masses and performance capabilities. Several researches[4][10] have been made to express the components' masses by their critical parameters. Bershadsky[4] documents a method to characterize the masses of drive components by use of a market search and curve-fitting of all the data to find a general equation that hinges upon the main parameters of the components. This thesis makes use of this method to estimate the masses of the drive components.

1.1 Drive components

1.1.1 Electric motors

Brushless Direct Current (BLDC) motors are the primary choice of electric motors for multirotor applications. This type of electric motors is more efficient than brushed configurations from the electrical-mechanical energy conversion point of view[4]. There are two types of BLDC motors; Outrunner (OR) and Inrunner (IR). The difference between these two types is that the OR configuration produces more torque than the IR configuration even though it covers more area. Consequently, OR motors are more suitable for large vehicles and IR motors are best for lighter and smaller vehicles.

The most important parameter of BLDC motors is the speed constant, K_v. The speed constant states how much RPM an electric motor can produce per

the voltage applied on it. It is measured in rpm/V. As an example, a BLDC motor with a low K_v value must spin faster than one with a higher K_v to produce the same amount of thrust but too high values of K_v may cause an inability to handle the loads at high throttle inputs. High K_v motors are preferable for high-maneuvering flights while low K_v motors mounted under a large radius/low pitch propeller are more efficient.

1.1.2 Electronic Speed Controllers (ESCs)

ESCs are the control units for electric motors. To change the speed of a motor, the corresponding ESC takes the given pulse width modulation signal and varies the switching rate of field effect transistors (FETs), the motor spins by the frequency of switching[4].

Electronic speed controllers are selected considering the parameter called maximum rated amperage, A_m, which describes how much current the ESC can withstand.

1.1.3 Batteries

Batteries are the source of energy for electric multirotor UAVs. The most common type of battery used for UAV applications is the Lithium-Polymer (LiPo) one. These type of compositions have specific energy values of one-tenth of gunpowder and one-hundredth of kerosene, which is up to 250 Wh/kg[4][16].

The selection of the battery for such applications depends on the battery's cell configuration, cell capacity and the nominal voltage value. The internal system of a battery consists several serial and parallel cells with corresponding cell capacities measured in mAh. Cell capacity combined with the internal system configuration gives information about the amount of current that can be supplied by the battery per hour. Because of that, the choice of the battery considering the amount of cell capacity and the configuration is significant for operation time goals. In addition, the propulsion and the other power sink systems must be fed by the battery with the adequate voltage to operate properly. Connecting the internal cells in series multiplies the voltage that the battery can supply while making these connections in parallel increases the total capacity of the battery.

As an example, a battery which has a configuration of 3S1P with cell capacity of 600 mAh and nominal voltage of 3.7 V/cell supplies a total of 11.1 V and has a total capacity of 600 mAh. If the configuration becomes 4S2P, the total capacity increases from 600 to 1200 mAh because of the parallel connection and the total voltage supply increases to 14.8 V as a result of increasing number of cells connected in series. A battery with a capacity of 1200 mAh is able to provide 1.2 A of current for one hour if fully discharged. Bershadsky states that decreasing the amount of discharge of a battery results in a longer battery life[4]. Manufacturers usually indicate the discharge rate of a battery by a parameter called "C-rating".

C-rating is the indicator of how much steady discharge a battery can provide. In numbers, a battery with a total capacity of 500 mAh and 20C is capable of providing 10A of current.

1.1.4 Propellers

Propellers are the most important aerodynamic components of multirotor UAVs. They are characterized by their radius, pitch and number of blades. Propeller pitch is described as the horizontal distance covered by the propeller when it has turned one full lap. These parameters have significant influences on the vehicle performance and they need to be taken into account carefully during the design process.

Furthermore, the material that the propeller is made of counts as another important consideration on the choice of propellers. Generally, UAV propellers are made of wood, plastic, nylon reinforced plastic or carbon fiber. The choice of the material is crucial not only on the mass problem but also affects the aerodynamic efficiency of the propeller. Stated by Harrington[11], propellers that are built by flexible materials tend to deflect from the plane of rotation at higher rotational speeds, which creates a declination on the produced thrust. During the propeller choice, this effect must also be considered.

1.2 Mass parametrization of drive components

Researches have been made to find analytic relationships between the specific parameters of the drive components that were introduced in the previous section and their masses. As mentioned before, this thesis makes use of the parametrization technique introduced by Bershadsky. This technique involves numerous searches on the market and collecting all the component data in order to illustrate them graphically to find an analytic relationship by curve-fitting techniques between the components mass and the specific parameter of the component[4]. Estimating the masses of the components is the key point on calculating the lift force needed to be produced while design process.

1.2.1 BLDC motor

Figure 1.1 illustrates the relationship between the speed constant of a motor and its mass both for IR and OR BLDC motors. As reported, 991 OR and 696 IR motors have been considered in this survey. The blue and red lines show the curve-fit of the data and an equation has been obtained. According to Bershadsky[4], the mass of the motor, in grams, can be predicted by

$$m_m = 10^{p_1} {K_v}^{p_2}, \tag{1.1}$$

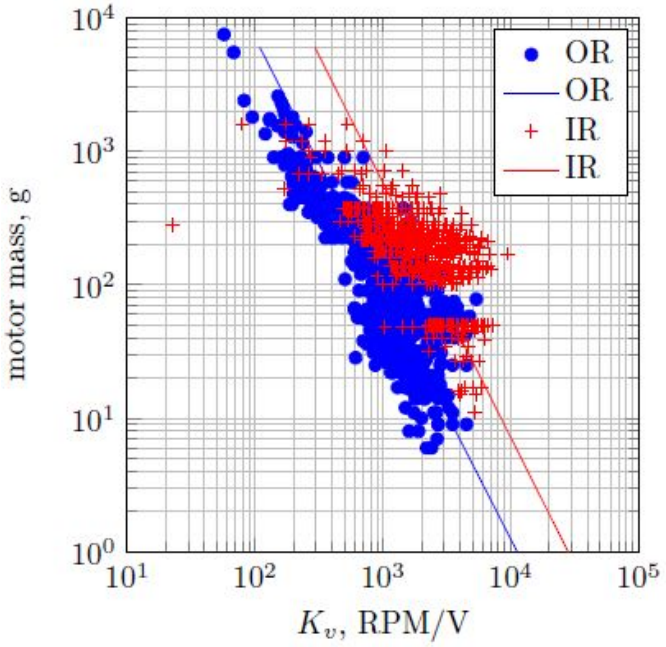

Figure 1.1: Motor speed constant vs. mass[4]

where coefficient p_1 is 4.0499 for OR motors and 4.4482 for IR motors and p_2 is -0.5329 for OR motors and -0.5242 for IR motors. It is also stated that the fit does not capture quite accurately the mass of the motors between 0 and 500 K_v, which are the mostly used type for "hobby-sized" vehicles[4]. In order to closely estimate the mass of the motors belonging to this range, a correction has been made in terms of curve-fitting for OR motors between 0 and 6000 K_v range. Figure 1.2 shows the K_v-to-mass relationship after modification.OR H line corresponds to the modified fit. In this thesis, the modified fit is used to estimate the OR motor masses.

1.2.2 ESC

The market survey done by Bershadsky includes 20 electronic speed controllers which have maximum rated amperage values up to 100A[4]. Figure 1.3 shows the relationship between the ESC A_m and its mass with the obtained fit.It is stated that the mass of the ESC, measured in grams, making use of its maximum rated amperage can be obtained by

$$m_e = 0.8421 A_m. \tag{1.2}$$

1.2.3 LiPo battery

Market search done by Bershadsky consists of 30 LiPo batteries which have internal cell configurations between two to six serial and one parallel[4]. A re-

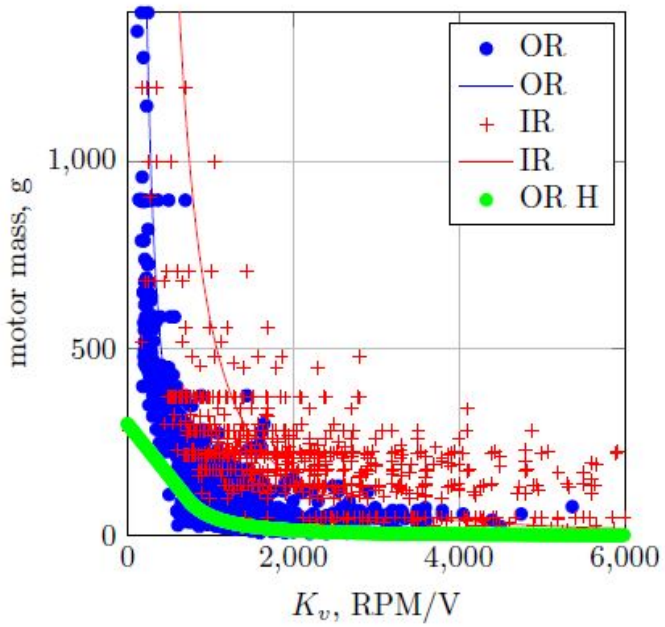

Figure 1.2: Motor speed constant vs. mass with modified OR fit[4]

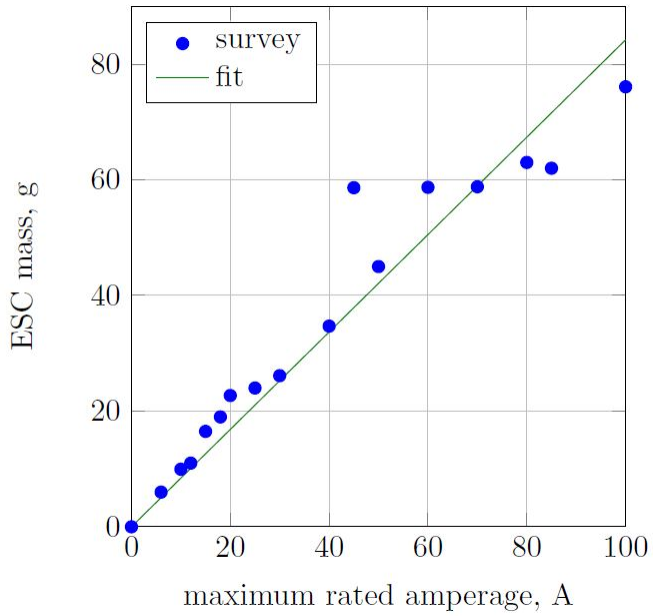

Figure 1.3: ESC maximum rated amperage vs. mass[4]

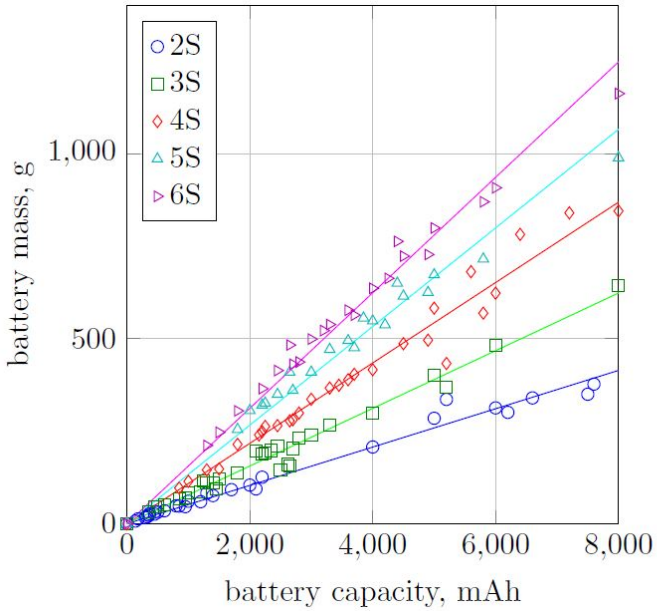

Figure 1.4: Battery capacity vs. mass[4]

lationship between the total capacity of the battery and the mass is found by curve-fitting. Figure 1.4 illustrates the market search results and the corresponding fits. As a result of the fitting process, an analytical equation that describes the mass of the battery, measured in grams, considering its cell configuration and total capacity has been found to be

$$m_b = (p_1 s + p_2)C, \tag{1.3}$$

where p_1 is 0.026373 and p_2 is 2.0499e-05. The variable s stands for the number of cells connected in series while C is the total capacity of the battery.

1.2.4 Propeller

Bershadsky states that about 30 propellers are surveyed for the mass estimation problem and Figure 1.5 is obtained, curve-fitting is used to obtain the relationship between the diameter of the propeller and its mass[4]. The propellers in this search are built by four different type of materials which are mentioned before; wood, plastic, nylon reinforced plastic and carbon fiber.

As a result of the curve-fitting process, the following equation is found to express the propeller mass in grams

$$m_p = p_1 D^2 + p_2 D + p_3. \tag{1.4}$$

Table 1.1 shows the values of the parameters in equation (1.4).

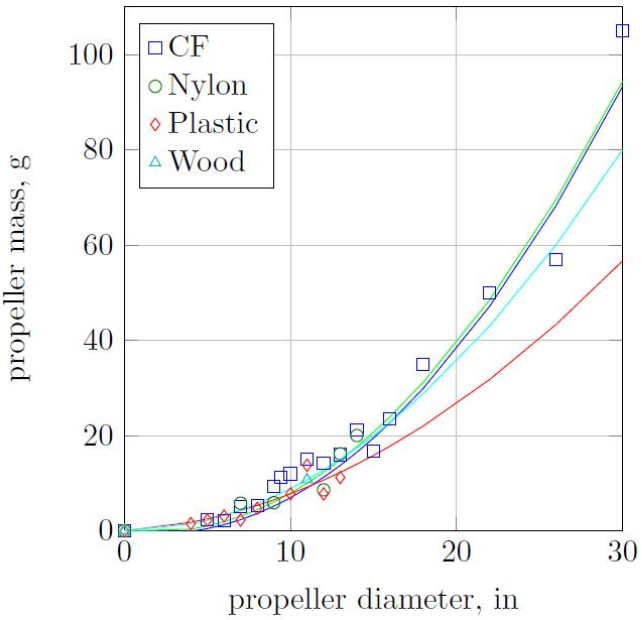

Figure 1.5: Propeller diameter vs. mass[4]

Material	p_1	p_2	p_3
Wood	0.08884	0	-1.0510
Plastic	0.05555	0.2216	-1.6
Nylon-reinforced plastic	0.1178	-0.3887	0.1685
Carbon fiber	0.1207	-0.5122	2.4553

Table 1.1: Parameters in equation (1.4) for different propeller materials

1.2.5 Mass breakdown

As mentioned previously, multirotor unmanned aerial vehicles have four significant drive components to considered in the design process. In addition to these components, there are several other parts that need to be counted while estimating the mass of the vehicle.

These other parts are named as *non-flight components* in this thesis. It means that these components are not critical in the flight process of the vehicle but their mass and also their need of electrical energy must be taken account in the process of design and optimization. The first part is structural part, which forms the base of the vehicle. Bershadsky states that, the structural mass of an unmanned aerial vehicle changes between 8% to 40% of its gross take-off weight[4]. To estimate the structural mass of the vehicle in design, the algorithm developed in this thesis does not use a constant ratio but offers a user-input option.

Second consideration is the wiring mass of the vehicle. Bershadsky reports that the wiring mass, which contains all the signal and power line masses, is found to be equal to 5% of GTOW of all multirotor UAVs[4]. This ratio is used in this thesis to estimate the wiring mass.

Lastly, the mass of avionics and payloads must be taken into account. As these parts are added externally without the need of mass estimation, this thesis offers to enter the mass data of avionics and payloads inside the estimation process. Also, for performance calculations, the current drain of these components has to be entered by the user.

Chapter 2

Propeller modeling

The design problem of a multirotor unmanned aerial vehicle mainly focuses on the performance capabilities of the vehicle. These capabilities greatly depend on the aerodynamic features of the propellers mounted on the vehicles. Therefore, the propeller characteristics must be modeled properly in order to estimate the performance capabilities of the vehicle in-design. In this chapter, a brief introduction of the aerodynamic theories implemented into the design tool is given and the geometrical parametrization of the propellers is introduced.

2.1 Rotor aerodynamics

Multirotor UAVs are vehicles with more than one rotor. Therefore, the aerodynamic theories that explain the rotor performance are applicable to multirotor vehicles. In this section, two fundamental theories are explained and eventually combined in order to evaluate the rotor performance characteristics. These two theories are:

- Momentum Theory
- Blade Element Theory

All presented theories in this section are for hover condition of a rotorcraft.

2.1.1 Momentum Theory

Momentum Theory is a theory presented by Glauert[9] built on the works done by Rankine[14] and Froude[7] for marine propellers. The theory presented in this section is taken from Leishman[13].

Momentum Theory is built on the assumption that the rotor can be idealized as an infinitesimally thin actuator disk which a pressure difference exists on. The

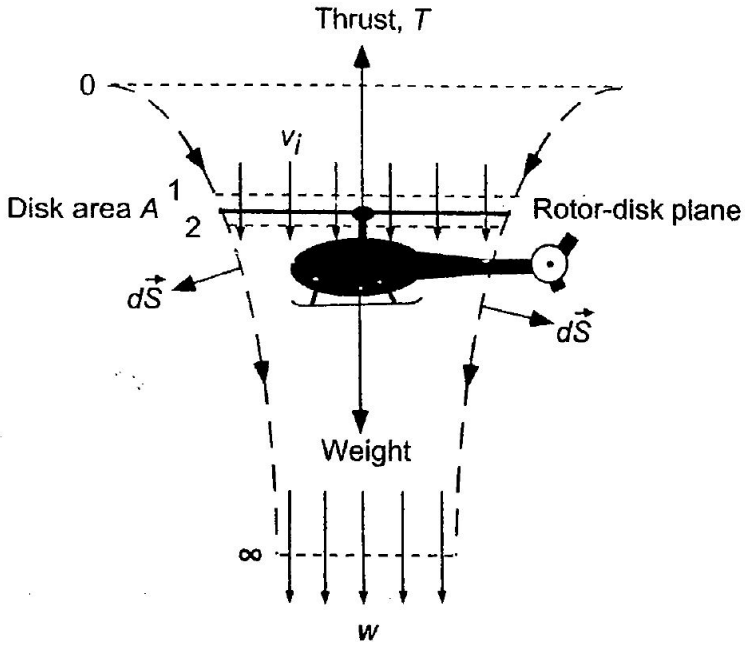

Figure 2.1: Flow model of a rotor in hovering flight[13]

flow model is assumed to be axisymmetric, one-dimensional, quasi-steady, incompressible and inviscid. Consequently, the conservation laws of mass, momentum and energy is applied to the finite control volume seen in Figure 2.1.

In Figure 2.1, cross-section 0 denotes the far upstream plane of the rotor, where the flow is stationary for hovering condition ($V_0 = 0$). The planes just above and below the actuator disk are denoted as cross-sections 1 and 2 respectively. Cross-section ∞ denotes the far wake and the area of the disk is represented with A. The velocity on the rotor disk which is the velocity imparted to the air in the control volume is called *induced velocity*, denoted as v_i. The velocity at the far wake is w.

From the conservation of mass and the assumption of quasi-steady flow, a constant mass flow rate present within the boundaries of the control volume. Therefore, the mass flow rate $\dot{m}$ in the control volume is

$$\dot{m} = \rho A_\infty w = \rho A_2 v_i = \rho A v_i. \tag{2.1}$$

The conservation of momentum states that in a control volume, the net force on the fluid is equal to the time-rate-of-change of fluid momentum out of the control volume. This relation is applicable between the rotor thrust T and the flow out of the control volume. Rotor thrust is found to be equal and opposite to the force applied on the fluid. Also in hovering flight, the flow far upstream of the rotor is quiescent. Above reasons simplify the momentum equation into a scalar form in hovering flight

$$T = \dot{m} w. \tag{2.2}$$

The energy gain of the fluid per unit time is equal to the work done on the rotor, which is indicated by the conservation law of the energy. Work done on the rotor is called the power consumed by the rotor and it is equal to Tv_i. Again considering the stationary flow at upstream in hovering condition, equation (2.3) is obtained.

$$Tv_i = \frac{1}{2}\dot{m}w^2. \tag{2.3}$$

Using equations (2.2) and (2.3), one can easily find that

$$w = 2v_i, \tag{2.4}$$

which means that the velocity induced by the rotor is equal to the half of the velocity at the far wake. This relationship helps to combine the thrust with the induced velocity

$$T = \dot{m}w = \dot{m}(2v_i) = 2\rho A{v_i}^2. \tag{2.5}$$

Equation (2.5) can be solved for v_i

$$v_i = \sqrt{\frac{T}{2\rho A}} = \sqrt{\left(\frac{T}{A}\right)\frac{1}{2\rho}}, \tag{2.6}$$

where the disk loading, T/A, defined as the ratio between the rotor thrust and rotor area, is a highly significant parameter in rotor analysis. Lower disk loading yields a higher hover efficiency in required power point of view.

The *ideal power*, which is the power completely induced since there are no considered viscous effects, is found to be

$$P = Tv_i = T\sqrt{\frac{T}{2\rho A}} = \frac{T^{3/2}}{\sqrt{2\rho A}}. \tag{2.7}$$

Alternatively,

$$P = Tv_i = 2\dot{m}{v_i}^2 = 2(\rho A v_i){v_i}^2 = 2\rho A{v_i}^3. \tag{2.8}$$

Obviously, the power required to hover depends on the induced velocity. In order to hover with minimum induced power at a constant thrust, the velocity induced by the rotor must be small. Using a large rotor in area yields a large mass flow rate through the disk and consequently, the induced velocity drops[13].

The nondimensional quantities that describes the rotor performance can be obtained by dividing the length variables by R and the velocity variables by ΩR where the rotor rotational speed is Ω and the rotor radius is R. Especially to compare different rotors, the nondimensional quantity called *inflow ratio*, denoted

as λ, is introduced. In hovering condition, the inflow ratio is equal to the ratio between the total velocity induced by the rotor and the blade tip speed, V_{tip}, which is equal to the rotor rotational speed times the rotor radius.

$$\lambda = \frac{v_i}{\Omega R} = \frac{v_i}{V_{tip}}. \tag{2.9}$$

Another quantity called *rotor thrust coefficient*, denoted as C_T, is also useful in rotor analysis.

$$C_T = \frac{T}{\rho A {V_{tip}}^2} = \frac{T}{\rho A \Omega^2 R^2}. \tag{2.10}$$

Equations (2.9) and (2.10) can be combined in a single equation to represent the relation between λ and C_T in hovering conditions;

$$\lambda = \sqrt{\frac{C_T}{2}}. \tag{2.11}$$

The rotor thrust coefficient and the inflow ratio representations of the Momentum Theory is used in Section 2.1.3 to estimate the performance of a rotor.

2.1.2 Blade Element Theory (BET)

Blade Element Theory divides the rotor blade into several adjoint sections. These sections are assumed to act as quasi-2-D airfoils that produce aerodynamic forces and moments without any interaction between them. Integrating the sectional airloads over the radius and averaging per one rotor revolution, the rotor global forces and moments can be obtained[13].

BET differs from Momentum Theory by considering the geometrical shape of the rotor blade in computations. While Momentum Theory accepts the rotor as a disk formed by an infinite number of blades with zero thickness, BET assumes that the rotor is formed by several blades. This approach makes it easy to demonstrate the distinction between the produced aerodynamic forces of moments by several rotors which have different rotor blades in shape.

The starting point of BET is the division of the rotor blade to multiple elements. In Figure 2.2, the three components of the flow velocity are shown. U_T is the tangential velocity component which is parallel to the rotor disk, U_P is the perpendicular velocity component which is normal to the rotor disk and U_R is the radial velocity component acting along the blade span. The lift is formed by the velocity and angle of attack normal to the leading edge of the blade; therefore, U_R is usually ignored in lift computations in hover condition. The resultant velocity U acting on the blade element is composed by U_T and U_P:

$$U = \sqrt{{U_T}^2 + {U_P}^2}. \tag{2.12}$$

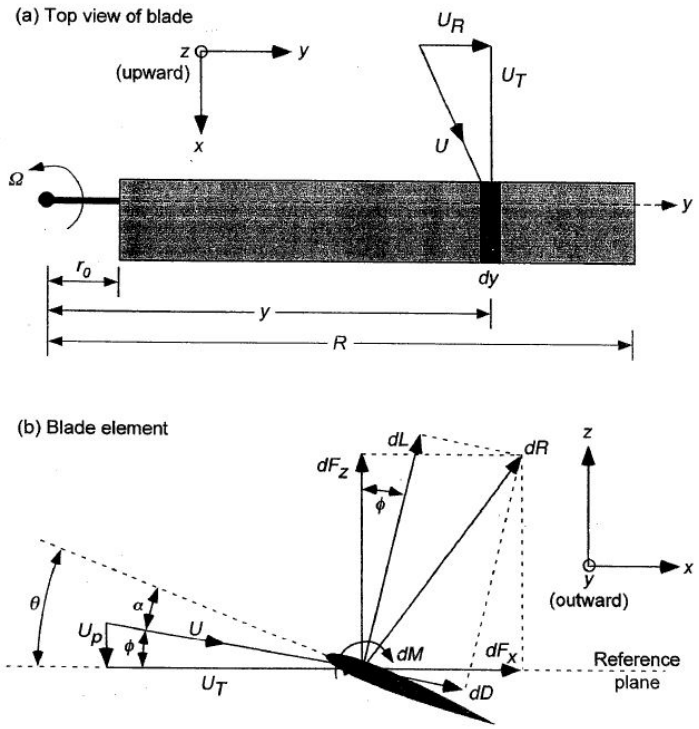

Figure 2.2: Flow velocities and aerodynamic setting of a blade element[13]

The in-plane velocity U_T on a blade element is formed by the blade rotation while the out-of-plane velocity U_P occurs due to the induced inflow.

$$U_T = \Omega y \tag{2.13}$$
$$U_P = v_i, \tag{2.14}$$

where Ω is the rotational speed of the rotor, y is the dimensional distance of the blade element from the axis of rotation and v_i is the induced velocity.

The inflow angle at the blade element, ϕ, and the effective angle of attack, α, result to be

$$\phi = \tan^{-1}\left(\frac{U_P}{U_T}\right) \approx \frac{U_P}{U_T} \tag{2.15}$$
$$\alpha = \theta - \phi, \tag{2.16}$$

where θ is the pitch angle at the blade element.

dL and dD, the resultant lift and drag increments per unit span on the blade element are

$$dL = \frac{1}{2}\rho U^2 c C_l dy \tag{2.17}$$
$$dD = \frac{1}{2}\rho U^2 c C_d dy, \tag{2.18}$$

where c is the local blade chord, C_l is the lift coefficient and C_d is the drag coefficient. The forces dF_z and dF_x in Figure 2.2 can be represented as

$$dF_z = dL\cos\phi - dD\sin\phi \tag{2.19}$$
$$dF_x = dL\sin\phi + dD\cos\phi \tag{2.20}$$

Herewith, the incremental thrust, torque and power of the rotor become

$$dT = N_b dF_z \tag{2.21}$$
$$dQ = N_b dF_x y \tag{2.22}$$
$$dP = N_b dF_x \Omega y, \tag{2.23}$$

where N_b is the number of blades forming the rotor.

Leishman[13] states that 3 additional assumptions can be made to simplify the theory:

1. $U_P \ll U_T$: The in-plane component of the velocity is much greater than the out-of-plane component. Therefore, the resultant velocity is $U = \sqrt{U_T^2 + U_P^2} \approx U_T$.

2. The induced angle ϕ is relatively a small angle. For this reason $\phi \approx U_P/U_T$, $\cos\phi \approx 1$ and $\sin\phi \approx \phi$.

3. The drag force is smaller than the lift force for at least one order of magnitude. So, the contribution $dD\sin\phi$ is negligible.

Furthermore, in hover condition the aerodynamic setting is axisymmetric and the blade azimuth angle does not affect the airloads. Using previously defined assumptions, equations (2.21), (2.22) and (2.23) can be rewritten as

$$dT = N_b dL \tag{2.24}$$
$$dQ = N_b(\phi dL + dD)y \tag{2.25}$$
$$dP = N_b\Omega(\phi dL + dD)y, \tag{2.26}$$

The inflow ratio λ and the solidity σ result to be

$$\lambda = \frac{v_i}{\Omega R} = \frac{v_i}{\Omega y}\left(\frac{\Omega y}{\Omega R}\right) = \frac{U_P}{U_T}\left(\frac{y}{R}\right) = \phi r \tag{2.27}$$
$$\sigma = \frac{N_b c}{\pi R}, \tag{2.28}$$

where $r = y/R$ is the nondimensional radial position. Solidity is described as the ratio between the blade area and the disk area of the rotor. Using this information and decomposing dL, the incremental rotor thrust coefficient dC_T can be represented as

$$dC_T = \frac{1}{2}\left(\frac{N_b c}{\pi R}\right) C_l r^2 dr = \frac{1}{2}\sigma C_l r^2 dr. \tag{2.29}$$

Equation (2.29) is stated as one of the most constitutive equations of the BET. The usage of equations (2.29) and (2.10) to calculate the inflow distribution on the rotor is described in the next section.

2.1.3 Blade Element Momentum Theory (BEMT)

Momentum Theory and BET differ in their approach to the rotor aerodynamic problem. In order to take advantage of both, the combined version of these theories is presented in literature. Leishman[13] states that the Blade Element Momentum Theory (BEMT) invokes the several equalities between the Momentum Theory and BET in order to compute the inflow characteristics of the rotor.

BEMT considers an annulus of the rotor disk and equates the incremental thrust coefficient representations of both theories considering it. The simple Momentum Theory assumptions with the BET assumption of no-mutual effects between successive blade elements are taken into account throughout the procedure. Equations (2.30) and (2.31) represents the incremental thrust coefficients for Momentum Theory and BET respectively for an annulus of the rotor disk.

$$dC_T = 4\lambda^2 r dr \tag{2.30}$$

$$dC_T = \frac{1}{2}\sigma C_{l_\alpha}(\theta r^2 - \lambda r)dr, \tag{2.31}$$

where σ is the solidity, r is the nondimensional radial position and dr is the nondimensional radial increment. Equations (2.30) and (2.31) provide an analytical starting point to the numerical analyses for the inflow ratio λ. The initial inflow ratio for the prescribed radial position can be found by solving the quadratic function arising from the equality. In hovering condition, the initial inflow ratio is

$$\lambda_i(r) = \frac{\sigma C_{l_\alpha}}{16}\left(\sqrt{1 + \frac{32}{\sigma C_{l_\alpha}}\theta r} - 1\right), \tag{2.32}$$

where C_{l_α} is the lift slope of the airfoil in use and θ is the blade twist of that radial position.

After the determination of the starting inflow value, the procedure continues by calculating the angle of attack, the aerodynamic coefficients and the relative velocity of the blade element. Again invoking the equality between the incremental thrust coefficient representations, a new inflow ratio can be obtained. New aerodynamic variables are computed using the found inflow ratio and the loop continues to find a final value for the inflow. The loop quits when the error between the successively found inflow values are below a certain threshold. Subsequently, the final aerodynamic forces and moments are computed to estimate the performance of the rotor.

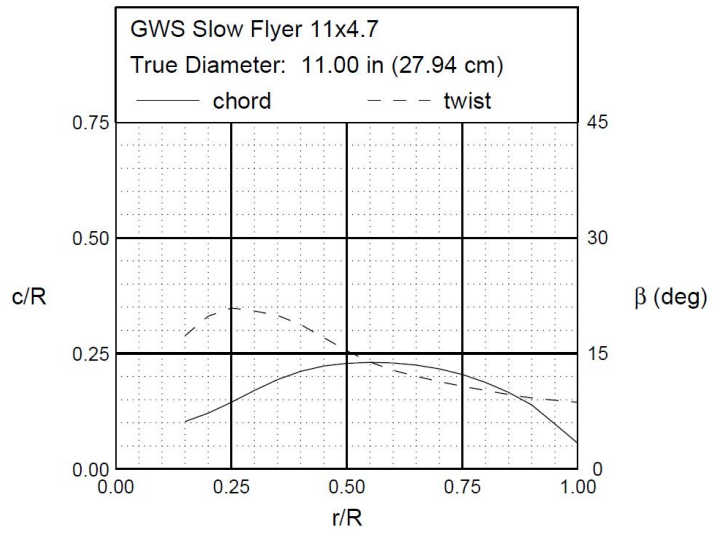

Figure 2.3: Geometric data of GWS SlowFly 11x4.7[5]

2.2 Geometric parametrization of the propeller

As mentioned previously, the propellers widely used on multirotor unmanned aerial vehicles are characterized by their radius, pitch and number of blades. Besides these parameters, the airfoil, the chord and the twist of the propeller must be described to make use of the aerodynamic theories. Having identified the radial distribution of the chord and the twist with the propeller airfoil, the calculation of the produced aerodynamic forces and moments becomes straightforward.

The proposed design and optimization tool in this thesis makes use of the chord and twist distributions of the GWS SlowFly propellers assuming constant airfoil of NACA0015 throughout the blade. The distributions and the analytic relationship between them and the propeller radius are documented by Brandt[5] and Bershadsky[4].

2.2.1 Chord & twist distribution

Brandt[5] reports a series of wind tunnel tests done on low Reynolds number propellers, which are widely used in multirotor applications, to document their performance characteristics. The dimensional data of the propellers have been measured throughout this procedure. Figure 2.3 shows the chord and twist distribution of a GWS SlowFly propeller.

The relationship between the blade radial position and its chord and twist at that exact position has been parametrized by Bershadsky[4]. This approach eases the use of propellers with different dimensions. Equation (2.33) describes the nondimensional chord while equation (2.34) demonstrates the physical twist

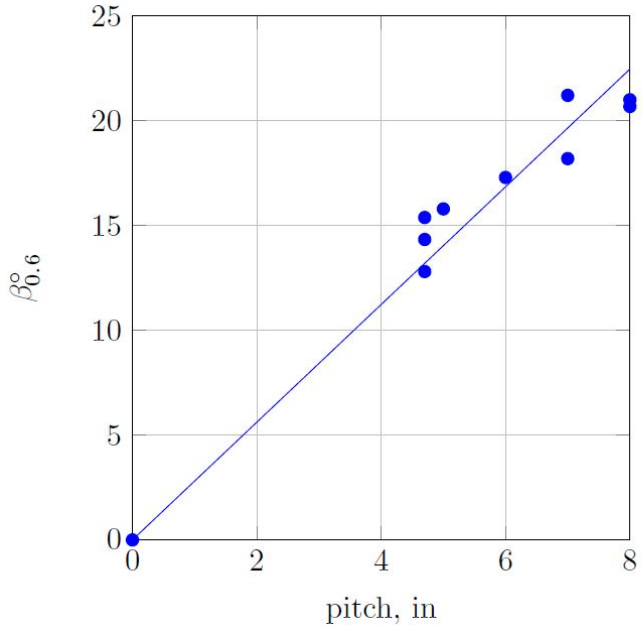

Figure 2.4: Twist of GWS propellers at 0.6R with respect to different propeller pitch values[4]

angle, measured in degrees, with respect to the nondimensional radial position:

$$c_R = p_1 {r_R}^3 + p_2 {r_R}^2 + p_3 r_R + p_4, \tag{2.33}$$

where p_1, p_2, p_3 and p_4 are equal to -0.2872, -0.1637, 0.4551 and 0.05648 respectively.

$$\beta = b_1 {r_R}^3 + b_2 {r_R}^2 + b_3 r_R + b_4, \tag{2.34}$$

where b_1, b_2, b_3 and b_4 are equal to 30.322, -64.731, 23.008 and 20.558 respectively.

Bershadsky[4] also states that the physical twist of a propeller blade depends on the propeller pitch value. Propeller pitch is known as the distance covered by the propeller along its rotation axis by one revolution, measured in inches. The twist of the propeller is effected by its pitch and needs to be scaled accordingly. The twist of GWS propellers at 0.6 nondimensional radial position for different values of propeller pitch are shown in Figure 2.4. Scaling the propeller twist with the propeller pitch indicates the correct twist distribution of the propeller in use and this procedure is vital to estimate the angle of attack of the blade accurately in every radial position.

2.2.2 Airfoil selection

Another aspect that has a significant effect on the performance of a propeller is its airfoil. The propellers in the UAV market differ a lot at airfoils in use;

furthermore, a lot of them do not contain a single airfoil but the shape varies throughout the blade. Hardened by these concerns, selecting a constant airfoil shape for all kind of modeled propellers in such a design tool is not the most accurate but the most ideal way. Different airfoil usage demands a wide range of airfoil data and implementation issues occur during the process. Neither the creation of such a data set nor the implementation of it inside the tool is the best choice from the computational point of view. Selecting an airfoil which one can access to its data easily is advantageous to reduce the effort of development. The NACA0015 airfoil is used in this thesis to model the propeller airfoil.

Constructing the propeller with an airfoil which is not the exact one used in the real situations causes the problem of inaccurate computation of the aerodynamic forces and moments. NACA0015 differs from most airfoils used on the propellers in the market from the camber point of view. NACA0015 is a camberless, symmetric airfoil whereas the propellers in the market are usually composed of airfoils with non-zero cambers, especially high-pitch propellers[4]. The computed thrust and power by the aerodynamic loop may become greatly inaccurate when the propeller modeled by the tool does not have a similar airfoil to NACA0015 in real.

Being easy-to-access and used by the ancestor tools makes NACA0015 a suitable choice for the developed tool in this thesis. The lift and drag coefficients of every single radial position is found by the corresponding angle of attack values considering NACA0015. The data are taken from Sheldhal[15] and a web database[1].

Chapter 3

Design and optimization tool

The tool developed in the thesis contains two major parts. The Forward Design tool (FDT) is the part which the drive component data are the main inputs. FDT aims to provide performance estimations about the vehicle in-design considering the provided data of the drive components. In addition, some more information about the vehicle must also be defined. Along with the performance capabilities, FDT has also the capability of analyzing the hover time variation of the vehicle considering a change in one of the drive component parameters. This sensitivity analysis is only by request of the user. In Section 3.1, FDT is explained with all its features and inside definitions.

The Drive Optimizer (DO) is the second part of the tool, in which the most significant inputs are the performance requirements. DO has the purpose of determining the best possible configuration of drive components that can achieve the desired performance characteristics. It can be simplified as a combination of multiple FDT loops which try to find a feasible solution considering the requirements. All algorithms are explained in Section 3.2.

3.1 Forward Design tool

This part of the tool is called "Forward Design" by reason of obtaining performance results with constrained drive components. It is a straightforward algorithm that uses an inductive approach. Figure 3.1 shows the overview of the FDT algorithm.

3.1.1 Inputs

Environment

FDT takes two inputs in the the environment section. These are the flight altitude above the ground and the take-off altitude, both measured in meters. FDT calculates the corresponding air density to take into account in BEMT algorithm.

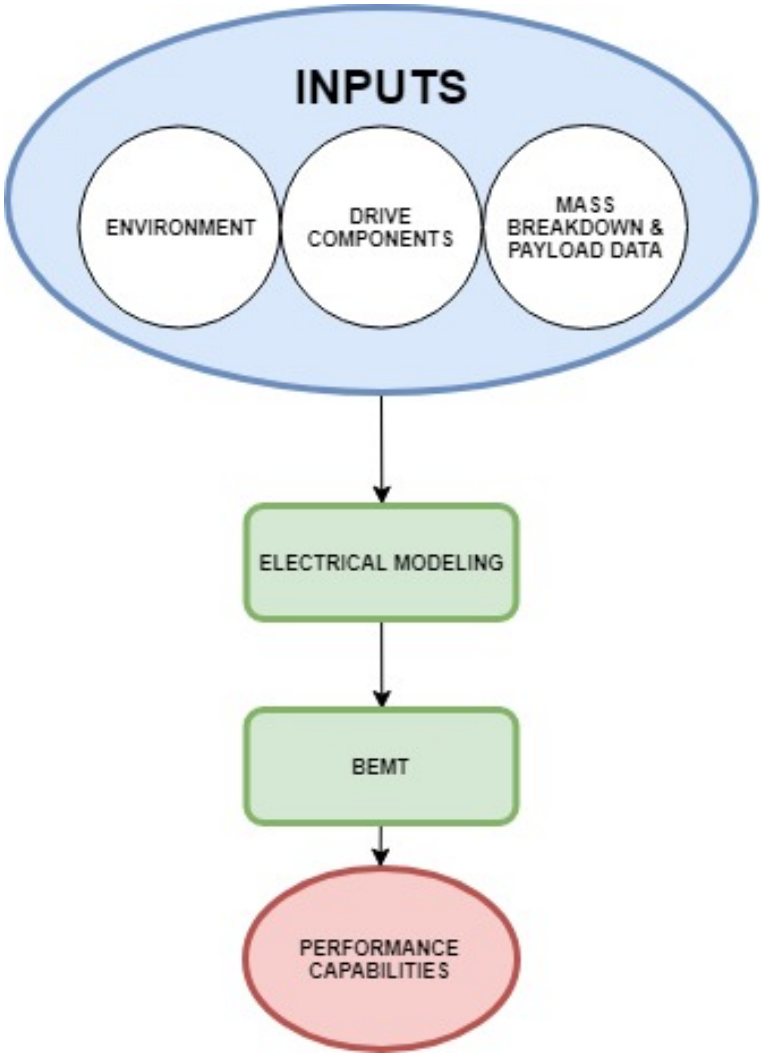

Figure 3.1: Overview of FDT

Drive components

Major inputs of FDT belong to this section. These inputs mainly describe the drive components that are used in the tool with the required additional data. The total list of the inputs in this section is

- Number of motors N_m
- Motor speed constant K_v
- Motor zero-load current I_0
- Motor type (IR/OR)
- ESC maximum rated amperage A_m
- Battery capacity per cell c
- Battery number of cells in serial connection s
- Battery number of cells in parallel connection p
- Battery nominal voltage V_b
- Propeller diameter D
- Propeller pitch p_p
- Number of blades per propeller N_b
- Propeller material

Mass breakdown & payload data

This section of the inputs is fundamental from the mass estimation point of view. FDT has two options in mass calculations; either the user can provide a gross take-off weight from the beginning of the analyses or FDT can estimate the total mass of the vehicle using the main drive component parameters that are explained in Chapter 1

Besides, mass estimation has to take the structural mass into account. Structural weight is described as a fraction to gross take-off weight in the process. This fraction must be defined by the user if the mass estimation of the vehicle is desired. Also, the user has to provide the weight and the current drain of the avionics and -if presents- the payload. Mass data must be considered while the estimation process and current drain have to be taken into account on endurance calculations.

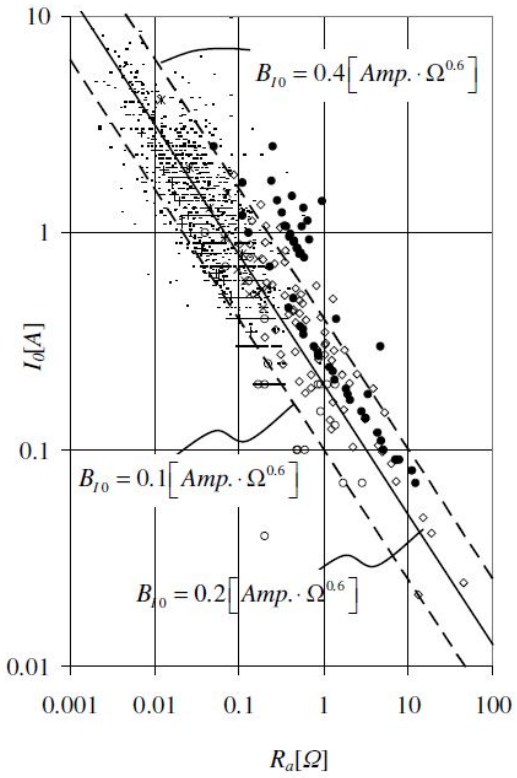

Figure 3.2: Motor internal resistance to zero-load current[10]

3.1.2 Electrical model

The electrical model of the vehicle must be specified to calculate the combined maximum capability of drive components. In order to model the circuit, the internal resistance of drive components must be found. Researches have been made in order to parametrize not only the mass but the internal resistance of such components. This thesis makes use of the parametrization process documented by Gur[10] and Ampatis[2].

BLDC motor

Gur[10] states that the internal resistance of a BLDC motor, R_{motor}, can be represented as a function of its speed constant K_v or zero-load current I_0. Figure 3.2, that shows the comparison of motor internal resistance to zero-load current of the motor, has been used to obtain equation (3.1) which expresses the relation between them analytically:

$$I_0 = \frac{B_0}{{R_{motor}}^{0.6}}. \tag{3.1}$$

The zero-load current parameter, B_0, is a representative parameter on estimating the internal resistance of a BLDC motor. B_0 is assumed to be equal to 0.25 A.$\Omega^{0.6}$ for this tool.

LiPo battery

Ampatis[2] reports that the total internal resistance of a battery, $R_{battery}$, is related with the cell configuration of the battery and the internal resistance per cell, R_{cell}. Equation (3.2) shows the analytical representation of the battery internal resistance.

$$R_{battery} = \frac{sR_{cell}}{p}. \tag{3.2}$$

R_{cell} is assumed to be equal to 10 mΩ for this tool.

ESC

Ampatis[2] documents that the internal resistance of an electronic speed controller depends on its transistor drain-to-source resistance, R_{DSON}, when it is in "ON" state. ESCs used with BLDC motors typically have three-state transistors to manage three phase currents. As a result, the internal resistance of an electronic speed controller, measured in mΩ, is

$$R_{ESC} = 3R_{DSON}. \tag{3.3}$$

It is stated that the value of R_{DSON} varies between 3 mΩ and 15 mΩ. This tool assumes that R_{DSON} is equal to 10 mΩ.

Wiring

The wiring resistance of the vehicle must also be considered. This tool assumes that the wiring is made of standard copper of 0.5 m length and 0.5 mm diameter.

Electric circuit

Figure 3.3 shows the electric circuit of the vehicle in-design.

FDT calculates the maximum angular velocity at which the motor is able to spin with considering the total battery voltage V_b, motor speed constant K_v, motor zero-load current I_0 and the total resistance of the circuit R_{total}. Ampatis[2] states that the maximum speed of a motor, measured in rpm, can be represented as

$$N_{max} = (V_b - I_0 R_{total})K_v, \tag{3.4}$$

and the total resistance of the circuit is given as

$$R_{total} = R_{battery} + R_{wiring} + \frac{R_{ESC} + R_{motor}}{N_m}. \tag{3.5}$$

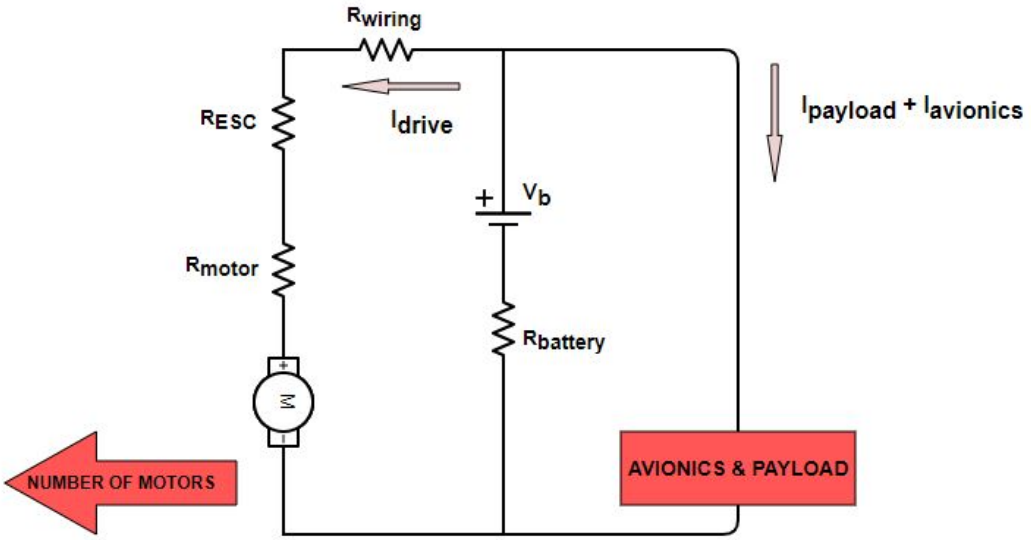

Figure 3.3: Circuit model of the developed tool

3.1.3 BEMT algorithm

The BEMT algorithm of the tool is based on the theory in Chapter 2. The algorithm tries to find the adequate angular velocity that the propellers must rotate with to produce the required thrust, equal to the gross take-off weight of the vehicle for hover condition.

The procedure of estimating the correct angular velocity is an iteration process of the throttle input d_t. The outer loop iterates d_t to find the corresponding angular velocity while the inner loop uses this velocity to make the computation of aerodynamic forces and moments produced by a single blade. The results are scaled by the number of blades on the propeller and the number of motors on the vehicle to find the total thrust and torque.

BEMT must be fed with the propeller characteristics. The chord and twist distributions with the other dimensional data, such as propeller pitch and diameter, are inserted into the algorithm for the calculations.

In addition, the gross take-off weight of the vehicle must be specified or estimated. It is needed to terminate the loop.

3.1.4 Performance analyses

The main assignment of FDT is to estimate the hover endurance t_h for the prescribed configuration. FDT computes the required angular velocity through the BEMT model in an iterative fashion and, using this information, the required

voltage for the motor is calculated considering the speed constant of the motor. The drive current, I_{drive}, is calculated using the angular velocity and torque computed through BEMT model. Combined with the current drain of the avionics and the payload, I_{drive} is used to compute the hovering time. t_h is found by equation (3.7)

$$I_{total} = I_{drive} + I_{payload} + I_{avionics} \tag{3.6}$$

$$t_h = C/I_{total}. \tag{3.7}$$

Bershadsky[4] reports that a discharge rate less than 100% for batteries is useful to maintain a longer battery life. FDT user can specify a discharge rate before the analyses. In this situation, the total capacity of the battery C is scaled by the discharge rate.

Hover analyses of FDT screens four outputs:

- Hover angular velocity [rad/s]
- Hover endurance [min]
- Hover current [A]
- Hover throttle input [%] .

Apart from hover analyses, FDT uses forward flight aerodynamics combined with the procedure described by Bershadsky[4]. For the specified forward flight inputs, which are the lower and upper bound for forward velocity and velocity increment, FDT computes the forward flight endurance and the corresponding range. The prescribed forward velocities are included inside the BEMT algorithm to take the axial flow effect into account. The analyses are constrained by the requirement that the vehicle is not allowed to lose altitude during the forward motion.

In forward flight, rotor pairs of the vehicle spin with different angular velocities to tilt the vehicle in the forward direction. This tilt develops a force that introduces an axial motion. Because of different angular velocities, FDT computes an average angular velocity for endurance calculations.

Forward flight analyses of FDT introduces five outputs for every forward velocity value:

- Vehicle tilt angle [deg]
- Flight time [min]
- Estimated range [m]
- Throttle input [%]
- Average angular velocity [rad/s] .

3.1.5 Sensitivity analyses

FDT has the option to calculate the sensitivity of the hover time considering the key parameters of the drive components and the gross take-off weight. The user can define an increment to one of the key parameters (or GTOW) and FDT calculates the hover time of the new configuration changing the initial parameter value.

If the increment is defined for one of the drive component parameters, the algorithm finds two new configurations; one with the initial value minus the increment and the other with the initial value plus the increment. If the gross take-off weight of the vehicle is constrained from the beginning, the algorithm does not estimate the mass of the component with the new parameter but uses the constant GTOW. If not, the mass of component is calculated again and the hover time is computed accordingly. To make the results reliable, it is useful to define the value of the increment as low as possible.

GTOW can also be used in the sensitivity analyses. If the user has started with a constant GTOW, it is possible to define an increment for GTOW and analyze the hover time sensitivity. FDT calculates the hover times of the two new configurations; one with GTOW minus the increment, the other with GTOW plus the increment. The algorithm estimates the change in hover time by the change in GTOW and screens the result.

The user can make sensitivity analyses with respect to:

- Motor speed constant K_v
- Propeller diameter D
- Propeller pitch p_p
- Battery capacity C
- Gross take-off weight .

3.2 Drive Optimizer

As mentioned previously, Drive Optimizer aims to find the best configuration of drive components to form the multirotor UAV considering the performance requirements. The performance requirements that can be specified for this tool are hover endurance t_h and maximum gross take-off weight W_{max}. DO tries to find the lightest vehicle which can hover more than t_h. Figure 3.4 shows the general algorithm of DO.

The configuration of drive components in DO is totally dependent on the key parameters which are described in Chapter 1. These parameters are iterated up to a specified limit until the desired performance is obtained. The performance calculations are executed by the BEMT algorithm.

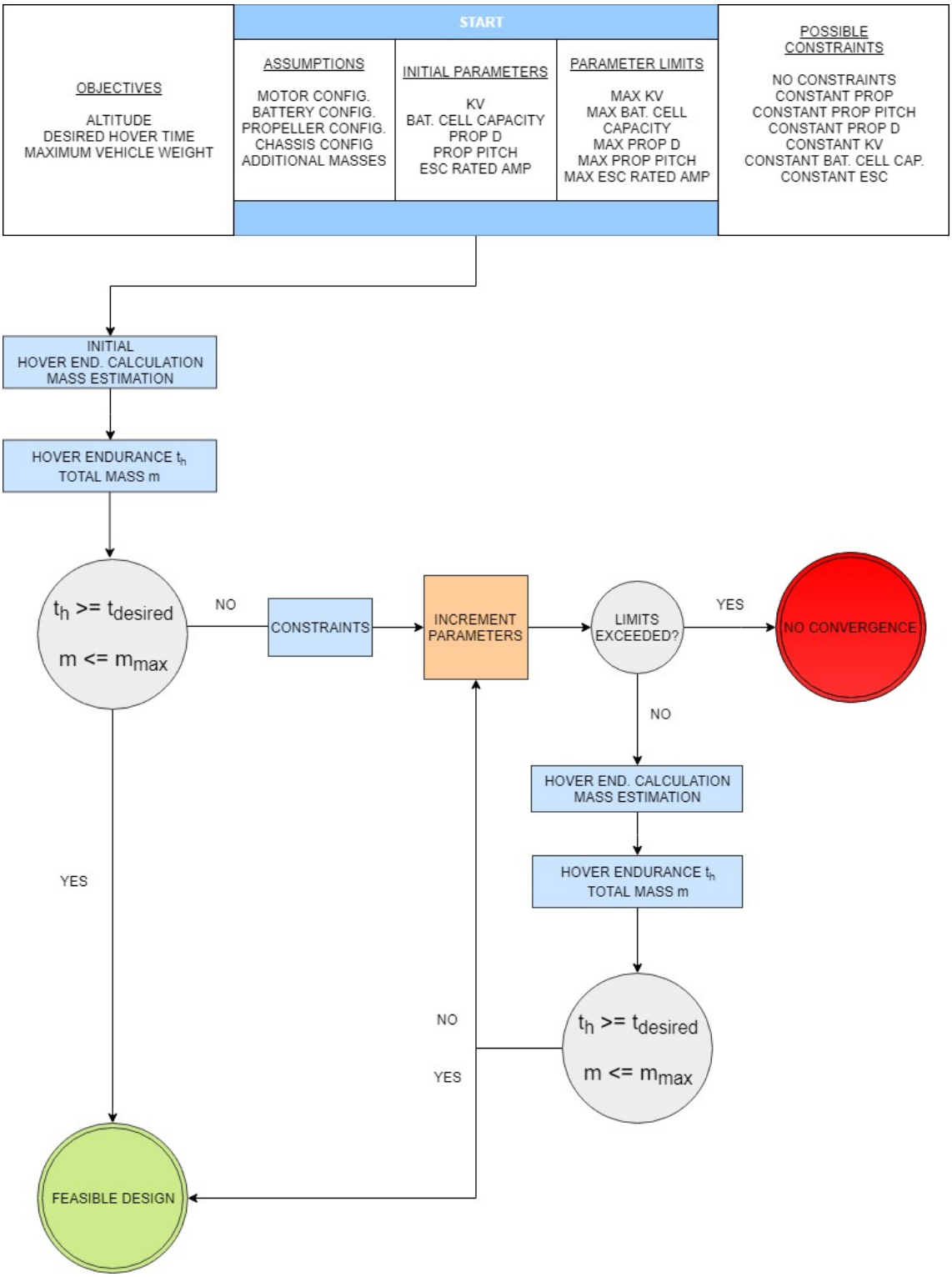

Figure 3.4: Overview of DO

3.2.1 Inputs

The input section of DO consists of five parts. These can be listed as

- Objectives
- Assumptions
- Initial parameters
- Parameter limits
- Constraints

Objectives

The objectives section contains three inputs, which are the flight altitude h, desired hover endurance t_h and the maximum gross take-off weight $GTOW_{max}$. The user defines these inputs considering the desired usage range of the vehicle in-design. The algorithm calculates the air density considering h and tries to find the configuration which can hover longer than t_h and weighs less than $GTOW_{max}$.

Assumptions

As in FDT, a part of the total configuration must be specified before the algorithm is executed. For example, the user has to define how many motors form the vehicle and how many blades form the propeller. Also, the battery configuration must be defined before (s, p and V) with the structural fraction of the vehicle and payload-avionics data.

Another aspect is the selection of the maximum allowable throttle input value for the hover condition. For example, assuming that the maximum allowable d_t is 80% for a generic multirotor, the selection of an upper boundary of 60% for the DO analyses allows the user to grant a future maneuverability margin of 20% d_t.

Initial parameters

The key parameters of the drive components are speed constant K_v for motors, propeller pitch p_p and diameter D for propellers, maximum rated amperage A_m for ESCs and capacity C for batteries by reason of mass estimation depends on these parameters. They must have starting values at the beginning and these are defined by the user. Apart from that, the user must also define the increments that the parameters are iterated accordingly.

Parameter limits

This input section consists in the limit values of the key parameters which the iteration takes place on until they reach these values. The ranges of the parameters is defined by the initial and limit values.

Constraints

DO has the capability to make seven kind of iterations. The user can either constraint a parameter or let the algorithm be free to iterate every parameter. The constraint options are:

- No constraints
- Constrained motor (constant K_v)
- Constrained battery (constant C)
- Constrained ESC (constant A_m)
- Constrained propeller diameter (constant D)
- Constrained propeller pitch (constant p_p)
- Constrained propeller (constant D and p_p)

For example, the user can make DO to find a configuration without constraining the drive components or a propeller configuration can be selected and used throughout the whole procedure.

3.2.2 Algorithm

The DO procedure starts with forming the electrical model as in FDT. Then the process continues with the computation of the mass of the vehicle and the hover endurance with the initial parameters using the BEMT model. If the algorithm finds that the initial configuration is able to hover longer than t_h and is lighter than W_{max}, the procedure stops.

On the contrary, the algorithm starts to iterate the parameters considering the increments defined for each parameter and the selected constraint type. As previously stated in Chapter 1, the mass of the drive components increases with increasing parameter value except for motors; the mass of the motor decreases with increasing speed constant. Because of that, the DO algorithm increases C, p_p and D while decreasing K_v. This is important in the range definition of the parameters; the user must select the initial values as the lower bounds and the limit values as the upper bounds, except for K_v: the initial value of K_v must be considered as the upper bound and the limit value as the lower bound.

Throughout the procedure, the algorithm calculates the gross take-off weight of the vehicle and hover endurance to compare with the objectives. The loop continues until the objectives are satisfied. If the configurations that are inside the parameter limits cannot achieve the prescribed objectives, the algorithm terminates. In this situation, the user must consider changing the configuration assumptions and the range of parameters. If a feasible configuration is found, DO asks the user whether to terminate the loop or not. The user has the option to continue iterating or end the process.

It may not always be possible to find the drive components with the exact values of parameters on the market. Considering this possibility, DO tries to define a range for K_v after finding the satisfying configuration. The configuration is assumed to be constrained except for the motor; the algorithm iterates K_v to find a lower bound which is useful for the user to select the motor comparing with the ones on the market.

3.3 Computational effort

Forward Design tool is a single run analysis tool that can perform 3 different analyses. A full run contains a single hover run, forward flight runs equal to the number of prescribed forward velocities and 5 sensitivity analyses. For example, a full run takes between 60 to 100 seconds depending on the given configuration of drive components, the mass estimation process, the selected forward flight velocity range and the prescribed increments for the sensitivity analyses. The main computational time is spent on the sensitivity analyses, which is - for a full run - equal to 80-90 % of the total time. Reducing the sensitivity increments reduces the computational effort significantly.

Drive Optimizer is a large mathematical computation model which forms its range for the drive component parameters according to user inputs. Computational effort significantly increases when the range of the parameters are too wide. As an example, the user can specify the range of K_v from 5000 rpm/V to 1000 rpm/V with an increment of 50 rpm/V. In this situation, the DO construct a set of 800 motors. Considering the others parameter ranges for the battery and the propellers, the total number of configuration sets increases rapidly and DO must perform hover analysis until a set meets the requirements. Defining a narrow range always decreases the computational time.

Furthermore, due to the desire of decreasing the computational effort, DO's BEMT algorithm divides the propeller blade to sections which are less than the FDT's BEMT algorithm number of division. While this difference only results in a change in hover endurance between 0.1-0.3 minute for most cases, it extremely decreases the computational time.

Chapter 4

Results

In this chapter, the results of the mass estimation models of Chapter 1 are compared with the real mass of the corresponding drive components. Furthermore, the available tools which are similar to FDT are introduced and performance results for different multirotor UAV configurations obtained by these tools are compared with the FDT results. Also, the FDT hover time results for specific multirotor configurations are compared with the experimental flight data of those vehicles and an example of the sensitivity analyses is presented for a generic multirotor.

Moreover, a set of already designed multirotor UAVs is used to validate the Drive Optimizer by taking their experimental endurance and weight data and using them as requirements inside the DO. The DO solutions are compared with the exact configurations of the vehicles.

4.1 Mass estimation survey

For the validation of the mass estimation models, the real mass data of several drive components and their calculated masses by the estimation model are compared. The results are shown in Table 4.1.

Considering the batteries, corresponding mass results are quite accurate and usable. Even though the percentage error is not adequately small, the propellers are light components and the difference between reported and calculated masses are not too large.

Estimation results for ESCs diverge from the real masses of the surveyed components. This is mainly due to the miniaturization, which is mainly making these components smaller at a very fast rate. Furthermore, the motor mass estimation process gives unreliable results. There is not any stationary margin between the real masses and the computed results. Most of the errors occur when the speed constant of the motor increases beyond 2000 rpm/V threshold. However, considering the motor and the ESC as a couple during the mass estimation process, the

Component	Parameter	Reported mass g	Calculated mass g	Error %
BL motor 1	K_v 2150 [rpm/V]	32	7.87	-75.4
BL motor 2	K_v 710 [rpm/V]	115.7	106.28	-8.1
BL motor 3	K_v 1450 [rpm/V]	22	21.76	-1.1
BL motor 4	K_v 2300 [rpm/V]	30	7.46	-75.1
BL motor 5	K_v 3100 [rpm/V]	13	5.07	-61
BL motor 6	K_v 980 [rpm/V]	44	62.16	41.3
BL motor 7	K_v 2280 [rpm/V]	15	7.5	-50
BL motor 8	K_v 2500 [rpm/V]	11	7.12	-35.2
ESC 1	A_m 30 [A]	11.4	25.26	121.5
ESC 2	A_m 30 [A]	9	25.26	180.6
ESC 3	A_m 35 [A]	8.5	29.47	246.7
ESC 4	A_m 20 [A]	2.5	16.84	573.6
Battery 1	C 950 [mAh] 3s1p	67.8	75.18	10.9
Battery 2	C 5200 [mAh] 3s1p	330	411.53	24.7
Battery 3	C 2200 [mAh] 3s1p	166	174.11	4.9
Battery 4	C 2650 [mAh] 4s1p	330	279.61	-15.2
Battery 5	C 5000 [mAh] 4s1p	462.8	527.56	14.0
Battery 6	C 8000 [mAh] 6s1p	1071	1266.07	18.2
Prop. 1	D 6.5 [in]	3.2	2.62	-18.1
Prop. 2	D 12 [in]	10.1	12.47	23.4
Prop. 3	D 5 [in]	5.4	1.17	-78.3
Prop. 4	D 7 [in]	4.3	3.22	-25.1

Table 4.1: Mass estimation survey

total calculated mass does not diverge widely away from the real mass.

4.2 Forward Design tool results

4.2.1 Design tools on the market

There are several tools considering the preliminary design of multirotor UAVs in the market. In this thesis, the tools called Electric Multirotor Sizing Tool (EMST) and eCalc are introduced and their performance results are compared with the FDT results.

EMST is developed by the Georgia Institute of Technology UAV Research Facility[8] and mainly contains every analysis that FDT is capable to perform. EMST has the ability to perform hover, forward flight and sensitivity analyses such as FDT. The tool is described by Bershadsky[4]. The unique ability of EMST is the parametrization of drive components; FDT makes use of the same technique as well. The major differences between EMST and FDT are the construction of

the electrical system and the electrical characteristic assumptions of the drive components. By reason of these aspects, the analyses performed by both tools give different results.

eCalc[6] is the most known online multirotor sizing tool. It has the capability to calculate the performance characteristics of a multirotor UAV with the requirement of the characteristics of the drive components, including their mass and electrical data, but has the unique option of selecting the drive components on the market by its own broad database of COTS components. A design process using eCalc is documented by Benito[3].

As it is obviously comprehensible, EMST and FDT use only the significant parameters of the drive components to estimate their mass and electrical characteristics while eCalc requires these data as inputs.

4.2.2 Comparison with ancestor tools

The comparison between the previously mentioned tools and FDT is made by selecting different configurations and obtaining corresponding results. Table 4.2 indicates the configurations for the analyses, Table 4.3 shows the hover endurance results and the differences between the tools for hover endurance results are designated in Table 4.4.

Vehicle	number of motors	K_v rpm/V	A_m A	D in	p_p in	s	p	C mAh	V_b V	GTOW g
UAV 1	4	920	30	9	4	4	1	5000	3.45	1250
UAV 2	4	350	30	13	4.5	6	1	4500	3.45	2935
UAV 3	4	950	30	9	4.5	3	1	5100	3.45	1282
UAV 4	4	1900	12	5	3	4	4	325	3.6	520
UAV 5	4	1000	30	9	4	4	1	5000	3.7	1300

Table 4.2: UAV configurations used in the survey

It is clear from the results that the difference between the tools is not constant for different configurations. However, for this set of configurations, FDT is closer to eCalc results than EMST in the sense of mean absolute difference.

The primary inference of this survey is that the parametrization of FDT and EMST is similar in nature but different in practice, especially for electrical system. Neither FDT nor EMST is closer to eCalc in every situation.

4.2.3 Comparison with experimental flight data

Table 4.5 shows the analysis results compared with the hover endurance results obtained by FDT. Vehicles used in this specific work are developed by Aerospace

Vehicle	FDT hover end. *min*	EMST hover end. *min*	eCalc hover end. *min*
UAV 1	19.9	21.5	20.1
UAV 2	13.0	12.3	12.0
UAV 3	18.6	15.9	16.5
UAV 4	10.0	8.9	10.7
UAV 5	13.0	10.9	13.6

Table 4.3: FDT hover endurance comparison with other tools

Vehicle	FDT-EMST diff. *%*	FDT-eCalc diff. *%*	EMST-eCalc diff. *%*
UAV 1	-7.44	-0.99	6.96
UAV 2	5.69	8.33	2.50
UAV 3	16.98	12.72	-3.63
UAV 4	12.35	-6.54	-16.82
UAV 5	18.18	-4.41	-19.11
mean abs. difference	12.12	6.59	9.80

Table 4.4: Hover endurance differences between the tools for the survey in Table 4.3

Systems and Control Laboratory(ASCL), which is one of the scientific laboratories of the Department of Aerospace Science and Technology of Politecnico di Milano and all reported data are experimentally obtained.

In addition, Table 4.6 indicates the eCalc hover endurance results for ASCL multirotor vehicles and the error between reported data and eCalc for these vehicles.

Vehicle	Reported hover endurance *min*	FDT hover endurance *min*	Error *%*
ANT-1	6	5.75	-4.1
ANT-1.1	8	7.4	-7.5
HEXA	15	13.7	-8.6
Quad-R2P	10	9.7	-3
Tilt-R2P	7.5	7.8	4
		mean abs. error	5.44

Table 4.5: FDT hover endurance results compared with experimental flight data

Vehicle	Reported hover endurance *min*	eCalc hover endurance *min*	Error *%*
ANT-1	6	6.8	13.3
ANT-1.1	8	7.6	-5
HEXA	15	11.6	-22.6
Quad-R2P	10	11.3	13
Tilt-R2P	7.5	7.6	1.3
		mean abs. error	11.04

Table 4.6: eCalc hover endurance results compared with experimental flight data

Even though FDT is closer to the exact results than eCalc, both tools are in the ±15% error margin. These results validate the hover calculations of FDT.

4.2.4 Forward flight comparison between FDT & EMST

The forward flight result scheme of FDT and EMST are equal in construction. Both tools calculate the flight endurance and range for specified forward velocities. Two different multirotor configurations are analyzed to compare the tools; the results are shown in Tables 4.7 and 4.8. These two vehicles are 3DR Iris+ and Quad Mini Generic which is developed by the Georgia Institute of Technology UAV Research Facility[8].

Forward velocity *m/s*	FDT flight end. *min*	FDT range *km*	EMST flight end. *min*	EMST range *km*	End. err. *%*	Range err. *%*
0.5	18.2	0.54	15.8	0.47	15.4	14.9
1	17.8	1.06	15.7	0.93	13.2	14.0
1.5	17.2	1.54	15.5	1.38	10.9	11.6
2	16.6	1.98	15.0	1.81	10.2	9.4
2.5	15.9	2.38	14.9	2.23	7.0	6.7
3	15.2	2.74	14.8	2.67	2.9	2.6
3.5	14.6	3.05	14.4	3.02	1.2	1.0
4	13.7	3.29	14.1	3.39	-2.9	-2.9
4.5	12.9	3.48	13.8	3.74	-6.8	-6.9
5	12.1	3.62	13.5	4.06	-10.7	-10.8
mean abs. error					8.12	8.08

Table 4.7: 3DR Iris+ forward flight comparison

4.2.5 Sensitivity analyses scheme

As previously mentioned in Chapter 3, FDT performs sensitivity analyses considering the drive component parameters for hover endurance. Table 4.9 shows an example scheme of the sensitivity outputs of FDT.

Incremental sensitivity indicates the alteration caused by the increase in the parameter value exactly in the amount of the increment Δ. For example, the

Forward velocity *m/s*	FDT flight end. *min*	FDT range *km*	EMST flight end. *min*	EMST range *km*	End. err. %	Range err. %
0.5	9.9	0.29	8.85	0.27	12.3	7.4
1	9.8	0.59	8.79	0.53	11.5	11.3
1.5	9.6	0.86	8.70	0.78	10.4	10.2
2	9.4	1.12	8.62	1.03	9.0	8.7
2.5	9.2	1.37	8.50	1.28	7.8	7.0
3	8.9	1.60	8.39	1.51	6.2	6.0
3.5	8.6	1.81	8.23	1.73	5.0	4.6
4	8.4	2.01	8.05	1.93	4.1	4.1
4.5	8.1	2.19	7.86	2.12	3.2	3.3
5	7.8	2.34	7.62	2.29	2.4	2.2
mean abs. error					7.19	6.48

Table 4.8: Quad Mini Generic forward flight comparison

Parameter	Δ	Unit sensitivity		Incremental sensitivity	
K_v	200	-0.00	*min/rpm/V*	-0.08	*min/200rpm/V*
D	0.5	-0.53	*min/in*	-0.26	*min/0.5in*
p_p	0.5	-0.17	*min/in*	-0.08	*min/0.5in*
C	350	0.01	*min/mAh*	2.12	*min/350mAh*
GTOW	50	-0.01	*min/g*	-0.26	*min/50g*

Table 4.9: Sensitivity analyses for ASCL ANT-1

hover endurance increases with increasing battery capacity and decreases while increasing the other parameters.

To validate the results of the sensitivity analyses, ANT-1 and ANT-1.1 are considered. These two vehicles differ only for used motors, battery, and the gross take-off weight. Corresponding increments for these parameters represents the configuration of ANT-1.1 The obtained endurance change is 1.78 minutes, which is close to the reported hover endurance difference of 2 minutes.

4.2.6 Reasons of inaccurate results

The majority of the errors of FDT is caused by its propeller parametrization. Previously discussed in Chapter 2, FDT uses the propeller parametrization described by Brandt[5] and Bershadsky[4], which is not always accurate for multirotor analyses because of the wide range of multirotor propellers.

Also, the airfoil selection is another reason behind large errors. The reasons for the deviation from exact results because of the airfoil assumption is already described in Chapter 2.

Furthermore, the estimation of the mass of the components is not always accurate due to the fact that the parametrization technique is a curve-fitting process. As already stated in Section 4.1, the estimation results sometimes diverge from

the real results. Moreover, internal resistance parametrization of the components sticks to constant parameters such as, e.g., B_0 and R_{DSON}. These assumptions are not accurate for all of the components on the market.

4.3 Drive Optimizer results

For DO results, three multirotor UAVs designed and built by ASCL are used. Taking as requirements the exact hover endurance and weight values of these vehicles, DO obtains configurations to compare with the real configuration of the vehicles. The assumptions which have been mentioned in Section 3.2.1 are made according to the original configuration of the vehicle such as, e.g., number of motors, battery serial and parallel connections and number of blades per propeller. DO is operated in "no constraint" mode, which means none of the drive components are assumed to be constant.

Tables 4.10, 4.11 and 4.12 show the parameters of the vehicles and the corresponding DO solutions with respect to the exact hover endurance and GTOW of the vehicles.

	ANT-R	DO
K_v [rpm/V]	2300	1900
A_m [A]	30	30
D [in]	5	4
p_p [in]	4.5	3
C [mAh]	2650	2150
t_h [min]	13.0	13.1
GTOW [g]	733	625

Table 4.10: ANT-R compared with DO results

Using the same assumptions of the vehicles, DO results correspond to the lightest configuration that can be used for the same performance characteristics. The found parameters do not match with the exact component parameters in every situation; however, they are adequately close. As mentioned in Section 4.2.6, due to the used technique for estimating the physical and electrical characteristics of the components, corresponding deviations between the real case and optimizer case is understandable. Further validation of the DO must be performed by constructing a multirotor UAV with the configuration obtained by the tool and testing for hover endurance and GTOW to acquire the error between the tool and experimental results.

	TILT-X	DO
K_v [rpm/V]	2150	2300
A_m [A]	30	30
D [in]	6.5	5
p_p [in]	3.5	3
C [mAh]	5000	4500
t_h [min]	12.5	12.6
GTOW [g]	1523	1300.5

Table 4.11: TILT-X compared with DO results

	CARRIER-1	DO
K_v [rpm/V]	1600	1000
A_m [A]	35	30
D [in]	6.5	6
p_p [in]	3.5	3
C [mAh]	8000	7900
t_h [min]	18.0	18.1
GTOW [g]	2900	2795

Table 4.12: CARRIER-1 compared with DO results

Another run for ANT-R is made in "constrained motor" mode. Table 4.13 represents the results.

	ANT-R	DO
K_v [rpm/V]	2300	2300
A_m [A]	30	30
D [in]	5	3.5
p_p [in]	4.5	3.5
C [mAh]	2650	2200
t_h [min]	13.0	13.1
GTOW [g]	733	618.7

Table 4.13: ANT-R compared with DO results operated in "constrained motor" mode

As can be seen from Table 4.13, in "constrained motor" mode, DO keeps the motor speed constant K_v fixed and runs the analyses accordingly.

As previously stated in Section 3.2.2, it is not always possible to match the DO solution with the COTS components, especially for BLDC motors. Table 4.14 shows an example of DO solution that reports a lower bound for K_v to grant a range for the user to choose from within. The requirements and assumptions are stated in Table 4.15.

	Exact solution	Lower bounded solution
K_v [rpm/V]	4000	3450
A_m [A]	10	10
D [in]	3	3
p_p [in]	3	3
C [mAh]	900	900
t_h [min]	10.1	10.5
GTOW [g]	214.6	224.6

Table 4.14: Lower bound example scheme of DO

min. t_h	max. GTOW	N_m	I_0	d_{tmax}	B	s	p	V_b
min	*g*		*A*	*%*				*V*
10	300	4	0.5	60	2	3	1	3.7

Table 4.15: Performance requirements and assumptions of lower bound example in Table 4.14

According to Table 4.14, the user can select the motors that have K_v values between 3450 rpm/V and 4000 rpm/V with 0.5 A of I_0 for the vehicle in-design.

Conclusions

In this thesis, a design and optimization tool for multirotor unmanned aerial vehicles has been presented.

In detail, the description of multirotor UAV drive components has been given and the parametrization techniques for these components with related aerodynamic theories have been introduced. Through these techniques and theories, the physical, aerodynamical and electrical characteristics of drive components are estimated.

A tool that has two parts which are using different approaches to design a multirotor UAV has been introduced. The results of the tool have been compared with experimental data and two other design tools on the market. Also, the part of the tool that uses a deductive approach has been compared with a basic design technique.

Future work

Possible directions for future work are listed below:

- The electrical system estimation can be further parametrized to represent the drive components more accurately.
- The fitting errors in the mass estimation process can be taken into account to provide confidence bounds in the analysis and optimization results.
- Additional concerns such as, e.g., climb and descent rate can be further implemented inside the Forward Design tool as performance analyses and the Drive Optimizer as requirements.
- A multirotor UAV can be built by the Drive Optimizer and tested to further validate the tool.

Bibliography

[1] Airfoil tools. http://www.airfoiltools.com/airfoil/details?airfoil=naca0015-il. Accessed: 2018.

[2] C. Ampatis and E. Papadopoulos. Parametric design and optimization of multi-rotor aerial vehicles. In *Applications of Mathematics and Informatics in Science and Engineering*, pages 1–25. Springer, 2014.

[3] J. A. Benito, G. Glez-de Rivera, J. Garrido, and R. Ponticelli. Design considerations of a small uav platform carrying medium payloads. In *Design of Circuits and Integrated Circuits (DCIS), 2014 Conference on*, pages 1–6. IEEE, 2014.

[4] D. Bershadsky, S. Haviland, and E. N. Johnson. Electric multirotor uav propulsion system sizing for performance prediction and design optimization. In *57th AIAA/ASCE/AHS/ASC Structures, Structural Dynamics, and Materials Conference*, page 0581, 2016.

[5] J. Brandt and M. Selig. Propeller performance data at low reynolds numbers. In *49th AIAA Aerospace Sciences Meeting including the New Horizons Forum and Aerospace Exposition*, page 1255, 2011.

[6] ecalc - drive calculator. https://ecalc.ch/. Accessed: 2018.

[7] R. E. Froude. On the part played in propulsion by differences of fluid pressure. *Trans. Inst. Naval Architects*, 30:390, 1889.

[8] Georgia institute of technology uav research facility. http://uavrf.gatech.edu/. Accessed: 2018.

[9] H. Glauert. Airplane propellers. In *Aerodynamic theory*, pages 169–360. Springer, 1935.

[10] O. Gur and A. Rosen. Optimizing electric propulsion systems for uavs. In *12th AIAA/ISSMO Multidisciplinary Analysis and Optimization Conference*, page 5916, 2008.

[11] A. M. Harrington. Optimal propulsion system design for a micro quad rotor. Master's thesis, Department of Aerospace Engineering, University of Maryland, College Park, MD, 2011.

[12] E. S. Latorre. Propulsion system optimization for an unmanned lightweight quadrotor. Master's thesis, Univ. Politec. de Catalunya, Master in Aerospace Science and Technology, 2011.

[13] G. J. Leishman. *Principles of Helicopter Aerodynamics*. Cambridge University Press, 2006.

[14] W. J. M. Rankine. On the mechanical principles of the action of propellers. *Transactions of the Institution of Naval Architects*, 6, 1865.

[15] R. E. Sheldahl. Aerodynamic characteristics of seven airfoil sections through 180 degrees angle of attack for use in aerodynamic analysis of vertical axis wind turbines. *SAND80-2114*, 1981.

[16] J.-M. Tarascon and M. Armand. Issues and challenges facing rechargeable lithium batteries. In *Materials For Sustainable Energy: A Collection of Peer-Reviewed Research and Review Articles from Nature Publishing Group*, pages 171–179. World Scientific, 2011.